Article

Wetting of Two-Component Drops: Marangoni Contraction Versus Autophobing

Michiel A. Hack,[*,||] Wojciech Kwieciński,[*,||] Olinka Ramírez-Soto,[*,||] Tim Segers, Stefan Karpitschka, E. Stefan Kooij, and Jacco H. Snoeijer

Read Online

ACCESS | 📊 Metrics & More | 📰 Article Recommendations | 🔘 Supporting Information

ABSTRACT: The wetting properties of multicomponent liquids are crucial to numerous industrial applications. The mechanisms that determine the contact angles for such liquids remain poorly understood, with many intricacies arising due to complex physical phenomena, for example, due to the presence of surfactants. Here, we consider two-component drops that consist of mixtures of vicinal alkanediols and water. These diols behave surfactant-like in water. However, the contact angles of such mixtures on solid substrates are surprisingly large. We experimentally reveal that the contact angle is determined by two separate mechanisms of completely different nature, namely, Marangoni contraction (hydrodynamic) and autophobing (molecular). The competition between these effects can even inhibit Marangoni contraction, highlighting the importance of molecular structures in physico-chemical hydrodynamics.

Marangoni contraction — autophobing

water + 1,2-alkanediol
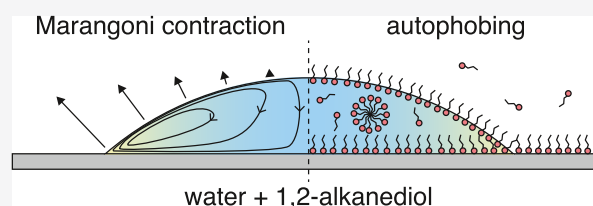
■ INTRODUCTION

Many industrial processes require a fundamental understanding of the wetting properties of liquids on solid surfaces.[1] Examples are inkjet printing,[2] oil recovery,[3] and lithography.[4] A key concept in the description of wetting is the contact angle θ, as defined in Figure 1. Properties of the liquid together with the surface chemistry of the solid determine the value of θ.[5,6] The wetting properties and contact angles of single-component liquids have been extensively studied.[7,8] However, a large number of industrial applications require mixtures of liquids[9] or the addition of a surfactant to enhance the spreading properties of a liquid.[10] For complex drops consisting of two or more components, the wetting properties are far from understood. The components may phase separate,[11,12] selectively evaporate,[13] emulsify,[14] and adsorb at interfaces,[15] and even gravity can play a role,[16,17] leading to intricate wetting properties on solid surfaces.

Here, we study the contact angle θ of multicomponent drops, where the less volatile component acts as a surfactant, on OH-terminated substrates that are fully wetted by water. Figure 1 shows the contact angle of drops consisting of water–1,2-hexanediol (1,2-HD) mixtures on a piranha solution-cleaned hydrophilic glass substrate (microscope coverslips, Menzel-Gläser) with minimal pinning. The reported angle is attained within seconds after deposition of the drop (see the Supporting Information). The key result of Figure 1 is that θ continually increases with the 1,2-HD mass fraction ϕ. This is surprising for two reasons. First, 1,2-HD has been shown to exhibit surfactant-like properties when mixed with water due to its amphiphilic molecular structure.[18–21] Increasing the mass fraction ϕ of 1,2-HD lowers the surface tension γ_{LV} (see the
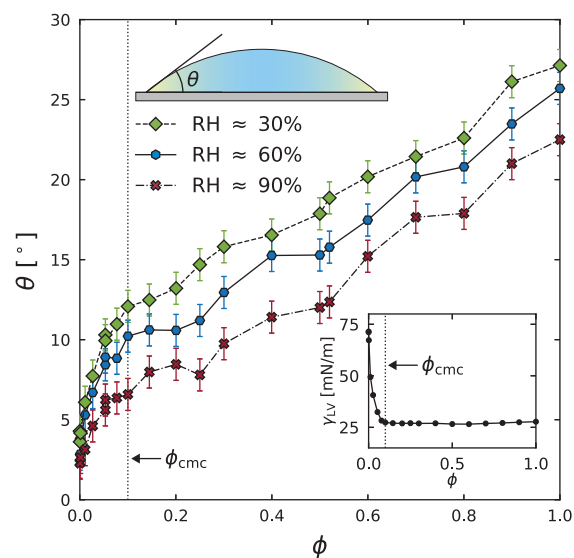

Figure 1. Contact angle (θ) of water–1,2-HD mixtures as a function of the mass fraction (ϕ) of 1,2-HD for various RH. The vertical dotted line indicates the cmc ($\phi_{cmc} \approx 0.1$). Schematic: Definition of θ. The mass fraction of 1,2-HD (yellow) is higher near the contact line due to selective evaporation. Inset: Surface tension (γ_{LV}) of water–1,2-HD mixtures, measured using the pendant drop method.
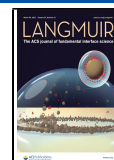
inset of Figure 1), which normally would lead to enhanced spreading. However, the opposite trend is found: θ increases with ϕ. A second surprise is that this increase continues above the critical micelle concentration (cmc) $\phi_{cmc} \approx 0.1$, even though γ_{LV} is constant in this range.[22] Here, we show that these unexpected features are the result of two mechanisms of different origins—one of hydrodynamic nature, Marangoni contraction, and the other of molecular nature, autophobing. This resolves the relation between two controversial models for Marangoni contraction[23-25] and, for the first time, describes quantitative limitations of the contracted state and its sensitivity to the molecular structure of the surface-active component.

■ RESULTS AND DISCUSSION

Marangoni Contraction. We first turn to the hydrodynamic mechanism, which is known as "Marangoni contraction."[24] Some multicomponent drops [e.g., water—1,2-propanediol (1,2-PrD) mixtures] can form non-zero contact angles on high-energy surfaces, even though the individual liquids themselves perfectly wet the surface at equilibrium (i.e., $\theta = 0°$).[9,23-26] There are two requirements that need to be satisfied for Marangoni contraction to occur: (i) one of the two liquids must be significantly more volatile than the other and (ii) the least volatile liquid should have the lowest surface tension of the two liquids. Selective evaporation at the contact line (where the evaporative flux is highest[27]) of the volatile component (typically water) then leads to a composition gradient in the drop and a surface tension gradient across the drop's interface. This in turn drives a Marangoni flow toward the center of the drop, which opposes the spreading of the drop, such that the drop is "contracted." The presence of Marangoni contraction invalidates Young's law, which only holds at equilibrium, that is, in the absence of flow,[5,7] and its effect is opposite to Marangoni spreading.[28]

Water—1,2-HD mixtures are expected to contract since 1,2-HD is considerably less volatile than water[12] and has a surface tension lower than that of water (see the inset of Figure 1). Figure 2a shows the flow field inside a $\phi = 0.08$ drop, as measured using high-resolution micro-particle image velocimetry. The blue line indicates the outer surface of the drop, and the contact line is located at $y = 0$. A strong inward flow exists near the surface of the drop, while an outward flow toward the contact line is observed in the bulk of the drop. This flow field is typical for Marangoni-contracted drops.[24] To further test the hypothesis that the increase of θ is due to Marangoni contraction, we varied the relative humidity (RH). A low RH enhances the evaporation that drives the flow inside the drop.[29] Indeed, Figure 1 shows that with a lower RH, the increase of θ is significantly enhanced, and for small ϕ, our data follows the Marangoni contraction scaling law (see the Supporting Information).[24] Therefore, we conclude that Marangoni contraction is responsible for the enhanced contact angle of water—1,2-HD drops at a small ϕ.

Marangoni contraction alone, however, cannot explain the full range of data in Figure 1. At $\phi = 1$, all surface tension gradients are removed, but nevertheless a large (non-zero) θ is observed. Furthermore, a monotonic increase of θ with ϕ is observed in Figure 1, even though a decrease in θ is expected for $\phi \gtrsim 0.6$, as is the case for 1,2-PrD which has been shown to contract due to smaller surface tension gradients and weaker internal flow.[24,25] Figure 2b shows the velocity field in a drop at $\phi = 0.22$, which is almost one order of magnitude smaller
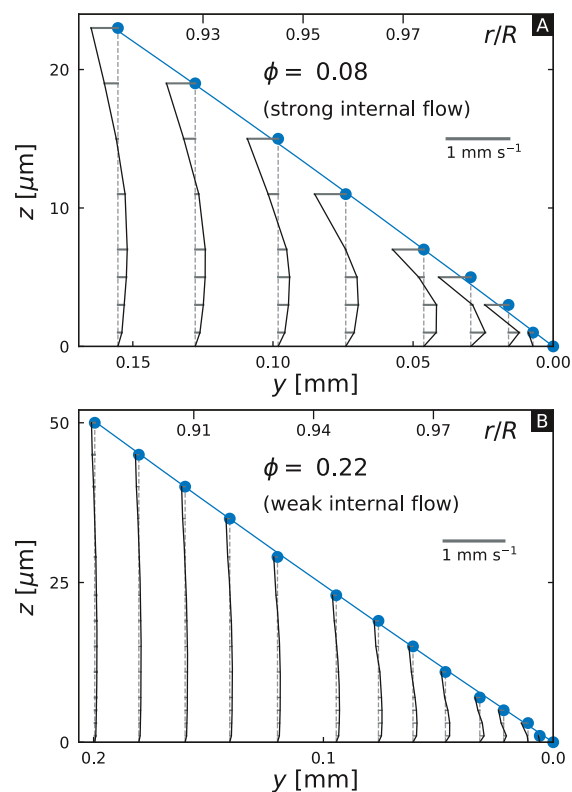

Figure 2. Horizontal velocity component in the drops measured using high-resolution micro-particle image velocimetry. The blue line indicates the outer surface of the drop. The horizontal lines indicate the velocity, where the direction is indicated by the location with respect to the vertical dashed line. (a) Velocity field for $\phi = 0.08$ and RH = 71% ($\theta = 9°$). (b) Velocity field for $\phi = 0.22$ and RH = 40% ($\theta = 14°$), which is significantly weaker than that in (a).

than the velocity in the $\phi = 0.08$ drop, which is too weak to sustain a contracted drop.

Autophobing. Another mechanism must be responsible for the large θ measured for a large ϕ. We recall the surfactant-like nature of 1,2-HD molecules. Some surfactant-containing liquids are known to be autophobic on selected substrates, a phenomenon where θ increases due to modification of the solid surface energy by a precursor of adsorbed surfactant molecules.[30-35] This layer of adsorbed molecules, which is of (quasi)monolayer thickness, is of different origin than the liquid precursor that is observed in "regular" wetting.[6] The surface energy of a precursor depends on RH, the composition of the drop, and the molecular nature of the adsorbing molecules.[10,36,37] To the best of our knowledge, autophobing and Marangoni contraction have never been reported to compete in a single multicomponent system. Importantly, the apparent shape of the drops is indistinguishable between the two states, but their dynamic behavior, especially their mobility and internal flows, is very different.[25]

To induce autophobing, surfactant molecules have to adsorb on the solid—liquid interface (inside the drop) or on the solid—vapor interface (the precursor outside the drop), resulting in an overall decrease of $\gamma_{SV} - \gamma_{SL}$, where γ_{SV} is the surface tension of the solid—vapor interface and γ_{SL} is the surface tension of the solid—liquid interface. In Figure 3a we report the adsorption properties of water—1,2-HD mixtures on the solid—vapor interface under ambient conditions, measured using ellipsometry.[38] Here, Γ is the number density of
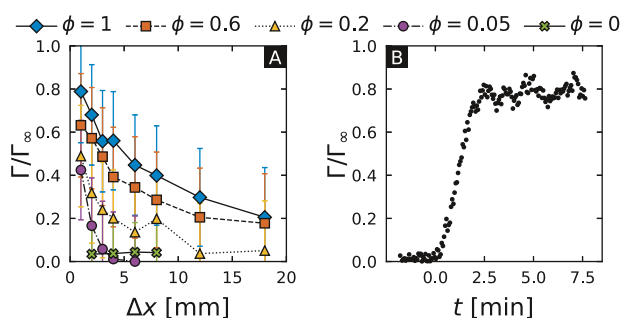
Figure 3. (a) Normalized adsorption density (Γ/Γ_∞) as a function of distance to the contact line (Δx) for several water−1,2-HD mixtures. (b) Temporal adsorption dynamics of pure 1,2-HD at $\Delta x \approx 5$ mm. The liquid is deposited at $t = 0$.

adsorbed 1,2-HD molecules, which we normalize by Γ_∞, the number density of adsorbed molecules corresponding to saturated coverage (measured in a closed chamber with saturated 1,2-HD vapor). All values of Γ/Γ_∞ were obtained after equilibrium was reached, as determined by measuring the temporal evolution of the adsorbed layer (Figure 3b), typically within a few minutes after deposition of the liquid. Complete desorption of the precursor upon removal of the drop typically takes an order of magnitude longer than the time it takes for the precursor to form (see the Supporting Information).

Figure 3a shows clear evidence of the adsorption of 1,2-HD molecules on the substrate. Additionally, it shows that Γ/Γ_∞ decreases both with the distance to the contact line Δx and with ϕ. This indicates that the concentration of 1,2-HD in the vapor surrounding the drop is of key importance to the equilibrium surface concentration of molecules adsorbed on the substrate. As we increase Δx or decrease ϕ, the concentration of 1,2-HD molecules in the vapor decreases. Hence, a lower number of 1,2-HD molecules is available in the vapor to adsorb on the substrate, while water becomes more abundant. Therefore, water coverage increases with increasing Δx and decreasing ϕ, resulting in a lower Γ/Γ_∞.

This indeed offers a direct explanation of the result in Figure 1, even when $\phi > \phi_{cmc}$, where θ increases with ϕ and decreases with RH. An increase in RH leads to a lower Γ/Γ_∞ due to the increased water coverage. Conversely, the 1,2-HD coverage increases by increasing ϕ. The adsorbed molecules change the surface energy of the substrate, making it more hydrophobic.[39] This offers clear and direct evidence that the contact angles of autophobed drops depend on the RH of the close surrounding of the contact line. We remind that the internal flow is very weak at large ϕ (Figure 2b), for which we thus expect to recover the true equilibrium contact angle. In Young's law, which remains valid at equilibrium in the presence of surfactants,[35] the increased hydrophobicity of the substrate is reflected in the $\gamma_{SV} - \gamma_{SL}$ term, which becomes smaller with increasing Γ/Γ_∞. Consequently, θ must increase, even though γ_{LV} remains constant above the cmc. This mechanism is reminiscent of the "modified Young's law" modeling approach used for multicomponent drops in refs.[23,25] Molecules may also adsorb on the solid−liquid interface, which we are unable to measure using our experimental setup.[40] Such adsorption, if dominant, could lower γ_{SL}, increase $\gamma_{SV} - \gamma_{SL}$, and thus lead to a decrease in θ. The increase of θ and the strong dependence of θ on RH (Figure 1) indicate that adsorption on the solid−vapor interface is dominant over adsorption on the solid−

liquid interface, leading to a decrease in $\gamma_{SV} - \gamma_{SL}$ and an increase in θ at large ϕ.

Contrary to many previous works on autophobing,[39−45] we do not see an initial spreading phase followed by a retraction to the quasi-steady θ (see the Supporting Information). This is likely due to the relatively high diffusion coefficient of 1,2-HD, which is a result of its small molecular size in comparison to other more common surfactants.[46] The region of the substrate that is sampled by the liquid in determining the stationary θ is no larger than 10 μm.[47] The timescale associated with forming the equilibrium adsorption layer within this region is smaller than the spreading timescale,[48] which is relatively long due to the high viscosity of 1,2-HD ($\eta \approx 82$ mPa·s[49]).

Effect of the Molecular Structure. Our experiments show that water−1,2-HD mixtures exhibit a competition between Marangoni contraction and autophobing. How generic is the observed competition between Marangoni contraction and authophobing and what is the influence of the surface activity $d\gamma_{LV}/d\phi$? Here, we address these questions by considering three shorter vicinal alkanediols: 1,2-PrD, 1,2-butanediol (1,2-BD), and 1,2-pentanediol (1,2-PeD), which have three, four, and five carbon atoms in their aliphatic chain, respectively. These diols are nonvolatile and have a low γ_{LV}.[50] The surfactant-like behavior (i.e., the surface activity $d\gamma_{LV}/d\phi$) depends on the length of the aliphatic chain. Short-chain alkanediols show weaker surfactant-like behavior (smaller $d\gamma_{LV}/d\phi$) due to the decreased hydrophobicity of the molecule.[50,51]

We study the properties of these diols using the same procedure as we used for 1,2-HD. Figure 4a shows θ as a function of ϕ at RH $\approx$ 60%. Starting at small ϕ, we see that all diols follow a universal curve. This is perfectly consistent with Marangoni contraction, as long as $d\gamma_{LV}/d\phi$ is sufficiently smaller than zero, and water remains more volatile in the mixture; the hydrodynamic mechanism remains insensitive to molecular details, while absolute flow velocities depend on the material parameters. Mixtures of other liquids are also expected to contract as long as their volatility and surface tension contrasts are in the same regime as those of water and carbon diols.[23] By contrast, the curves start to diverge and the length of the aliphatic chain matters for larger ϕ—consistent with autophobing. The longest diol studied here, 1,2-HD, exhibits strong autophobing behavior. As we move to short-chain diols, the autophobing strength becomes smaller, indicated by smaller values of θ at $\phi = 1$. Additionally, Figure 4a shows that Marangoni contraction is the dominant mechanism up to a larger ϕ for shorter diols. While for 1,2-HD, autophobing is dominant starting from $\phi \approx 0.3$, for 1,2-PrD, by contrast, the full range of ϕ is consistent with Marangoni contraction—there is no autophobing at all. Hence, a higher surface activity does not necessarily lead to stronger Marangoni contraction. In fact, the surface activity of the molecules may inhibit contraction, leading to autophobed drops. For example, at large ϕ, 1,2-HD (highest $d\gamma_{LV}/d\phi$) shows the strongest autophobing, whereas 1,2-PrD (lowest $d\gamma_{LV}/d\phi$) drops are contracted. Thus, our results show that, in addition to the two requirements listed above, there is a third requirement that needs to be satisfied for drops to contract: the contact angle achievable by Marangoni contraction needs to be larger than the microscopic contact angle as governed by molecular forces. However, the microscopic angle may be larger than zero.

All four molecules adsorb on the substrate, as seen from the ellipsometry measurements presented in Figure 4b. The
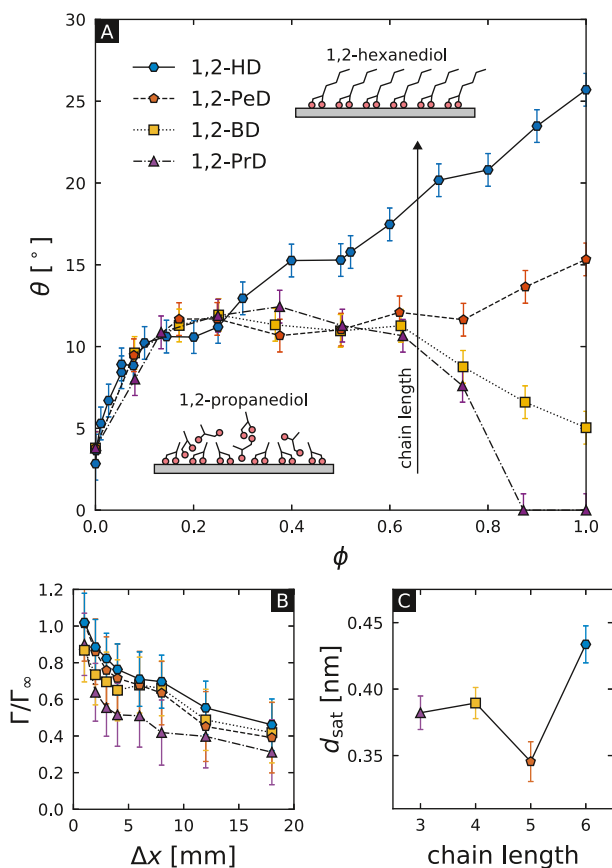
Figure 4. (a) Contact angle (θ) as a function of mass fraction (ϕ) for several mixtures of water and vicinal alkanediols (RH = 60%). The schematics show the structure of adsorbed 1,2-PrD molecules and 1,2-HD molecules. (b) Normalized adsorption density (Γ/Γ_∞) as a function of distance to the contact line (Δx). (c) Thickness of the saturated film (d_{sat}) for several vicinal alkanediols.

reduced autophobing strength of the shorter diols is caused by the shorter hydrophobic chain in these molecules. The distance between the hydrophilic and hydrophobic parts of the molecule is smaller in shorter-chain molecules, meaning that the polar nature of the hydroxyl groups becomes more relevant for the surface energy of an adsorbed layer of a short-chain molecule such as 1,2-PrD. The result is a more hydrophilic surface and therefore a smaller θ. Figure 4b shows that all diols studied here adsorb onto the substrate with similar Γ/Γ_∞. However, as shown in Figure 4c, not all adsorb in the same way as 1,2-HD. Despite their smaller size, the saturated thickness d_{sat} of 1,2-PrD and 1,2-BD is larger than that of 1,2-PeD and only slightly smaller than that of 1,2-HD, suggesting that they do not form monolayers (an estimate of the size of each molecule is given in the Supporting Information) since a monotonic increase in d_{sat} with the chain length is expected if monolayers are formed. Their hydroxyl groups remain partially exposed, allowing them to form disordered multilayered structures (see the schematic in Figure 4a) similar to layers of adsorbed water molecules.[52] Hence, they do not strongly affect the surface energy. By contrast, 1,2-PeD and 1,2-HD likely adsorb in a monolayer structure (see the schematic in Figure 4a), indicated by the increasing d_{sat} between 1,2-PeD and 1,2-HD in Figure 4c and the decrease in d_{sat} between 1,2-PrD and 1,2-PeD. This means that their long aliphatic chains are exposed, increasing the

hydrophobicity of the surface. Therefore, autophobing occurs at large ϕ for molecules with a long aliphatic chain due to the strong effect of the adsorbed molecules on the surface energy of the solid. By contrast, adsorbed molecules with a short aliphatic chain have little effect on the surface energy of the solid, and Marangoni contraction dominates over the full range of ϕ. One can thus tune θ over a large range by selecting the correct diol and a particular combination of ϕ and RH.

CONCLUSIONS

Our results reveal that Marangoni contraction and autophobing both provide valid descriptions for the wetting of two-component drops, albeit in different regimes. A minute change in one of the control parameters is sufficient to change the dominant wetting mechanism. While the visual appearance of drops in either of the two wetting states is indistinguishable, Figure 2 demonstrates a strong difference in their internal flows. We have shown (Figures 1 and 4a) that Marangoni contraction is possible only if the microscopic contact angle, as governed by molecular forces, is smaller than the angle achievable by contraction. Additionally, we show (Figure 2) that the internal flows should be used to determine the state of a drop rather than the contact angle or the apparent drop shape. By systematically changing the molecular structure of the volatile liquid, we show that a higher surface activity $d\gamma_{LV}/d\phi$ does not necessarily lead to stronger Marangoni contraction. In fact, excessive surface activity may inhibit contraction and lead to drops whose contact angle is governed by molecular forces. Hence, the chemical structure of the liquid needs to be taken into account when designing multicomponent drop systems with specific properties. Importantly, these mechanisms are generic and expected to be present in most mixtures containing (volatile) surfactant-like liquids (e.g., single alcohols).

Marangoni-contracted drops are attractive for technological applications due to their high mobility,[23,25,53] which is suppressed for drops in the autophobing or partial wetting states. Our result may also be of interest to applications that require high contact angles of drops consisting of low surface tension liquids, such as inkjet printing[54] or semiconductor processing.[9]

EXPERIMENTAL METHODS

Contact Angle Measurements. The contact angle θ was determined from the side-view images (obtained using a Ximea XiQ MQ013MG-ON camera with Zeiss Makro-Planar 1:2.8 f = 60 mm lens with Olympus ILP-2 light source). We determined θ by fitting a circle to the drop interface and a straight line to the substrate. The height H and base radius R of the drop are extracted from the circle fit and used to calculate the contact angle using $\theta = 2\tan^{-1}(H/R)$. The uncertainty in the contact angle, which originates from the pixel error and small variations in time (see Figure S1), is estimated to be $\pm 1°$. The RH was controlled using a home-built apparatus (for details see ref 55) and was constantly monitored along with temperature T during the measurement using a sensor (Honeywell HIH6130) in the setup. Example measurements of the time evolution of θ for ϕ = 0.08 and ϕ = 1 are shown in the Supporting Information.

Surface Tension Measurements. The surface tension measurements were performed using the pendant drop method.[56] For each aqueous solution of 1,2-HD, the surface tension of 10 drops of 2.5 μL was measured (T = 20 °C, RH = 45%), with 10 images collected for each drop over a period of 1 s. The surface tensions γ_{LV} reported in the inset of Figure 1 are an average of these measurements (i.e., 100 images per datapoint), with an average error of 0.57 mN/m.

Micro-particle Image Velocimetry Measurements. The flow velocities within evaporating binary drops of 1,2-HD and water were quantified by micro-particle image velocimetry. We used fluorescent polystyrene microspheres (Thermo Fisher Scientific F8809, 0.2 μm diameter, stock solution concentration 2% w/v) as tracers, with a mass fraction of 7.8×10^{-5} of the particle stock solution in the final mixture. The particles within the drops were visualized with an inverted epifluorescence microscope (Nikon Eclipse Ti2), equipped with a water immersion objective (Nikon CFI APO LWD 20× WI) with a numerical aperture of 0.95. Thin correlation depths (i.e., high plane selectivity) require diffraction-limited imaging. To achieve this not only close to the substrate but also in the bulk fluid, the refractive index of the immersion medium has to be close to that of the working medium, for which water immersion objectives are ideally suited. The focal plane was parallel to the substrate and moved in the vertical direction with the closed-loop focusing stage of the microscope. The time required to switch between planes was less than 100 ms. For each z-plane, a sequence of approximately 500 frames was recorded with a high-speed camera (Phantom VEO 4K 990L, imaging speed at 900−1000 fps). Thus, the time required for a full z-scan was on the order of approximately 10 s, much shorter than the time scale on which the flow velocities change for a quasi-stationary drop. This was checked by comparing data from successive upward and downward scans. To evaluate the flow velocities, the images were analyzed with an in-house developed cross-correlation based algorithm with adaptive interrogation window sizes and correlation averaging over approximately 100 frames. The analysis was implemented through the Python API of Tensor Flow to enable fast computation on graphics processing units. Example velocity fields in the z-plane are shown in the Supporting Information. The velocities presented in Figure 2 were obtained by azimuthally averaging over approximately 100 μm. Additionally, simultaneous shadowgraphy of the drop contour was performed to record the contact angle with a second camera (Point Grey Grasshopper2, imaging speed at 27 fps) through a macro lens (Thorlabs Bi-Telecentric lens, 1.0×, working distance 62.2 mm). Experiments were conducted in a humidity-controlled chamber mounted on top of the microscope. As substrates, we used piranha-cleaned microscope coverslips (Menzel Gläser).

Ellipsometry Measurements. The ellipsometry measurements (J. A. Woolam Co. VB-400-VASE ellipsometer with WVASE32 software) were performed on 2×2 cm^2 piranha solution-cleaned silicon (100) substrates (Okmetic) in ambient conditions ($T = 21$ °C, RH = $40 \pm 5\%$). The thickness d of the layer of adsorbed molecules was obtained by fitting the obtained ellipsometric spectrum to a model of a surface composed of a silicon substrate with a native oxide layer and the Cauchy layer on top. The thickness of the native oxide layer (typically 1.8 nm for these substrates) was determined for each substrate separately before performing the adsorption experiments. The Cauchy layer is an empirical model for the dependence of the refractive index on the wavelength of a dielectric layer

$$n(\lambda) = A + B/\lambda^2 + C/\lambda^4 + \dots \tag{1}$$

where n is the refractive index, λ is the wavelength of the light that is used, and A, B, and C are the material-dependent empirical coefficients.[57] Here, we used the values $A = 1.45$, $B = 0.1$, and $C = 0$, and all other higher order terms were set to zero.

During the measurement, the substrate is vertically placed above a Teflon container. A sketch of this configuration is available in the Supporting Information. A dynamic scan (3.5 eV, 75°) is used to resolve the adsorption of molecules over time. The measurement spot is located at a distance $\Delta x = 1$ mm from the liquid interface and has a diameter of approximately 1 mm. The obtained thickness is an average over the area of the measurement spot. To obtain the thickness of the adsorbed layer, we perform a measurement of the ellipsometric spectrum (1.2−4.5 eV, 75°), once the dynamic measurement indicates that the adsorption has reached equilibrium. The normalized adsorption density Γ/Γ_∞ is calculated from the thickness using $\Gamma/\Gamma_\infty = d/d_{sat}$. The value of d_{sat}, the thickness of the adsorbed film under saturated vapor conditions, is measured in a separate experiment in a closed chamber. The uncertainty in the ellipsometry measurements originates from the uncertainty in the native oxide layer thickness and the uncertainty in the Cauchy layer fit which is used to determine the adsorbed layer thickness.

The substrate on which the adsorption is measured is never in direct contact with the liquid. A similar technique was used by Novotny and Marmur.[38] This means that all measurements only take into account the molecules that are transported across the vapor phase separating the substrate and liquid. We compare the measurement with a gap (i.e., the case where no direct contact between the substrate and the liquid exists) to one without a gap (i.e., the case where direct contact between the substrate and liquid exists; the drop was placed directly on the substrate) in the Supporting Information. Within the error margin, there is no significant difference between the two measurements, indicating that the bulk of molecules adsorbed on the solid are transported across the vapor, and not, for instance, by fluid flow in a precursor film on the substrate.

■ ASSOCIATED CONTENT

ⓢ Supporting Information

The Supporting Information is available free of charge at https://pubs.acs.org/doi/10.1021/acs.langmuir.0c03571.

Contact angle, micro-particle velocimetry, and ellipsometry measurements; Marangoni contraction scaling law; and estimates of the molecular size of the different alkanediols (PDF)

■ AUTHOR INFORMATION

Corresponding Authors

Michiel A. Hack − *Physics of Fluids Group, Max Planck Center for Complex Fluid Dynamics, Faculty of Science and Technology, University of Twente, 7500 AE Enschede, The Netherlands;* ⓞ orcid.org/0000-0002-6229-8012; Email: m.a.hack@utwente.nl

Wojciech Kwieciński − *Physics of Interfaces and Nanomaterials Group, MESA+ Institute for Nanotechnology, University of Twente, 7500 AE Enschede, The Netherlands;* ⓞ orcid.org/0000-0002-0532-638X; Email: w.kwiecinski@utwente.nl

Olinka Ramírez-Soto − *Max Planck Institute for Dynamics and Self-Organization, 37077 Göttingen, Germany;* Email: olinka.ramirez@ds.mpg.de

Authors

Tim Segers − *Physics of Fluids Group, Max Planck Center for Complex Fluid Dynamics, Faculty of Science and Technology, University of Twente, 7500 AE Enschede, The Netherlands*

Stefan Karpitschka − *Max Planck Institute for Dynamics and Self-Organization, 37077 Göttingen, Germany*

E. Stefan Kooij − *Physics of Interfaces and Nanomaterials Group, MESA+ Institute for Nanotechnology, University of Twente, 7500 AE Enschede, The Netherlands;* ⓞ orcid.org/0000-0002-0049-4907

Jacco H. Snoeijer − *Physics of Fluids Group, Max Planck Center for Complex Fluid Dynamics, Faculty of Science and Technology, University of Twente, 7500 AE Enschede, The Netherlands*

Complete contact information is available at:
https://pubs.acs.org/10.1021/acs.langmuir.0c03571

Author Contributions

‖M.A.H., W.K., and O.R.-S. contributed equally

Notes

The authors declare no competing financial interest.

REFERENCES

(1) Starov, V. M.; Butt, H.-J. Editorial overview: Worldwide increasing interest in wetting phenomena. *Curr. Opin. Colloid Interface Sci.* **2018**, *36*, A1−A4.

(2) Wijshoff, H. The dynamics of the piezo inkjet printhead operation. *Phys. Rep.* **2010**, *491*, 77−177.

(3) Haagh, M. E. J.; Schilderink, N.; Mugele, F.; Duits, M. H. G. Wetting of mineral surfaces by fatty-acid-laden oil and brine: carbonate effect at elevated temperature. *Energy Fuels* **2019**, *33*, 9446−9456.

(4) Winkels, K. G.; Peters, I. R.; Evangelista, F.; Riepen, M.; Daerr, A.; Limat, L.; Snoeijer, J. H. Receding contact lines: from sliding drops to immersion lithography. *Eur. Phys. J. Spec. Top.* **2011**, *192*, 195−205.

(5) Young, T. An Essay on the Cohesion of Fluids. *Philos. Trans. R. Soc. London* **1805**, *95*, 65−87.

(6) Bonn, D.; Eggers, J.; Indekeu, J.; Meunier, J.; Rolley, E. Wetting and spreading. *Rev. Mod. Phys.* **2009**, *81*, 739−805.

(7) de Gennes, P.-G.; Brochard-Wyart, F.; Quéré, D. *Capillarity and Wetting Phenomena: Drops, Bubbles, Pearls, Waves*; Springer: New York, 2004; pp 35−38.

(8) Drelich, J. W.; Boinovich, L.; Chibowski, E.; Della Volpe, C.; Hołysz, L.; Marmur, A.; Siboni, S. Contact angles: history of over 200 years of open questions. *Surf. Innovations* **2020**, *8*, 3−27.

(9) Leenaars, A. F. M.; Huethorst, J. A. M.; van Oekel, J. J. Marangoni drying: a new extremely clean drying process. *Langmuir* **1990**, *6*, 1701−1703.

(10) Matar, O. K.; Craster, R. V. Dynamics of surfactant-assisted spreading. *Soft Matter* **2009**, *5*, 3801−3809.

(11) Tan, H.; Diddens, C.; Lv, P.; Kuerten, J. G. M.; Zhang, X.; Lohse, D. Evaporation-triggered microdroplet nucleation and the four life phases of an evaaporating Ouzo drop. *Proc. Natl. Acad. Sci. U.S.A.* **2016**, *113*, 8642−8647.

(12) Li, Y.; Lv, P.; Diddens, C.; Tan, H.; Wijshoff, H.; Versluis, M.; Lohse, D. Evaporation-triggered segregation of sessile binary droplets. *Phys. Rev. Lett.* **2018**, *120*, 224501.

(13) Sefiane, K.; David, S.; Shanahan, M. E. R. Wetting and evaporation of binary mixture drops. *J. Phys. Chem. B* **2008**, *112*, 11317−11323.

(14) Keiser, L.; Bense, H.; Colinet, P.; Bico, J.; Reyssat, E. Marangoni Bursting: Evaporation-Induced Emulsification of Binary Mixtures on a Liquid Layer. *Phys. Rev. Lett.* **2017**, *118*, 074504.

(15) Kim, H.; Boulogne, F.; Um, E.; Jacobi, I.; Button, E.; Stone, H. A. Controlled uniform coating from the interplay of Marangoni flows and surface-adsorbed macromolecules. *Phys. Rev. Lett.* **2016**, *116*, 124501.

(16) Edwards, A. M. J.; Atkinson, P. S.; Cheung, C. S.; Liang, H.; Fairhurst, D. J.; Ouali, F. F. Density-Driven Flows in Evaporating Binary Liquid Droplets. *Phys. Rev. Lett.* **2018**, *121*, 184501.

(17) Li, Y.; Diddens, C.; Lv, P.; Wijshoff, H.; Versluis, M.; Lohse, D. Gravitational Effect in Evaporating Binary Microdroplets. *Phys. Rev. Lett.* **2019**, *122*, 114501.

(18) Hajji, S. M.; Errahmani, M. B.; Coudert, R.; Durand, R. R.; Cao, A.; Taillandier, E. A comparative study of hexanediol-1,2 and octanetriol-1,2,3 in aqueous solutions by different physical techniques. *J. Phys. Chem.* **1989**, *93*, 4819−4824.

(19) Frindi, M.; Michels, B.; Zana, R. Ultrasonic absorption studies of surfactant exchange between micelles and bulk phase in aqueous micellar solutions of nonionic surfactants with short alkyl chains 1. 1,2-hexanediol and 1,2,3-octanetriol. *J. Phys. Chem.* **1991**, *95*, 4832−4837.

(20) Székely, N. K.; Almásy, L.; Rădulescu, A.; Rosta, L. Small-angle neutron scattering study of aqueous solutions of pentanediol and hexanediol. *J. Appl. Crystallogr.* **2007**, *40*, s307−s311.

(21) Tan, Y. H.; Finch, J. A. Frothers and gas dispersion: a review of the structure-property function relationship. *Physicochem. Probl. Miner. Process.* **2018**, *54*, 40−53.

(22) Romero, C. M.; Páez, M. S.; Miranda, J. A.; Hernández, D. J.; Oviedo, L. E. Effect of temperature on the surface tension of diluted aqueous solutions of 1,2-hexanediol, 1,5-hexanediol, 1,6-hexanediol and 2,5-hexanediol. *Fluid Phase Equilib.* **2007**, *258*, 67−72.

(23) Cira, N. J.; Benusiglio, A.; Prakash, M. Vapour-mediated sensing and motility in two-component droplets. *Nature* **2015**, *519*, 446−450.

(24) Karpitschka, S.; Liebig, F.; Riegler, H. Marangoni contraction of evaporating sessile droplets of binary mixtures. *Langmuir* **2017**, *33*, 4682−4687.

(25) Benusiglio, A.; Cira, N. J.; Prakash, M. Two-component marangoni-contracted droplets: friction and shape. *Soft Matter* **2018**, *14*, 7724−7730.

(26) Marra, J.; Huethorst, J. A. M. Physical principles of Marangoni drying. *Langmuir* **1991**, *7*, 2748−2755.

(27) Deegan, R. D.; Bakajin, O.; Dupont, T. F.; Huber, G.; Nagel, S. R.; Witten, T. A. Capillary flow as the cause of ring stains from dried liquid drops. *Nature* **1997**, *389*, 827−829.

(28) Mouat, A. P.; Wood, C. E.; Pye, J. E.; Burton, J. C. Tuning Contact Line Dynamics and Deposition Patterns in Volatile Liquid Mixtures. *Phys. Rev. Lett.* **2020**, *124*, 064502.

(29) Semenov, S.; Trybala, A.; Rubio, R. G.; Kovalchuk, N.; Starov, V.; Velarde, M. G. Simultaneous spreading and evaporation: recent developments. *Adv. Colloid Interface Sci.* **2014**, *206*, 382−398.

(30) Scales, P. J.; Grieser, F.; Furlong, D. N.; Healy, T. W. Contact angle changes for hydrophobic and hydrophilic surfaces induced by nonionic surfactants. *Colloids Surf.* **1986**, *21*, 55−68.

(31) Zhu, B.-Y.; Gu, T. Surfactant adsorption at solid-liquid interfaces. *Adv. Colloid Interface Sci.* **1991**, *37*, 1−32.

(32) Rupprecht, H.; Gu, T. Structure of adsorption layers of ionic surfactants at the solid/liquid interface. *Colloid Polym. Sci.* **1991**, *269*, 506−522.

(33) Birch, W. R.; Knewtson, M. A.; Garoff, S.; Suter, R. M.; Satija, S. The molecular stucture of autophobed monolayers and precursing films of a cationic surfactant on the silicon oxide/silicon surface. *Colloids Surf., A* **1994**, *89*, 145−155.

(34) Birch, W. R.; Knewtson, M. A.; Garoff, S.; Suter, R. M.; Satija, S. Structure of precursing thin films of an anionic surfactant on a silicon oxide/silicon surface. *Langmuir* **1995**, *11*, 48−56.

(35) Thiele, U.; Snoeijer, J. H.; Trinschek, S.; John, K. Equilibrium contact angle and adsorption layer properties with surfactants. *Langmuir* **2018**, *34*, 7210−7221.

(36) Afsar-Siddiqui, A. B.; Luckham, P. F.; Matar, O. K. Dewetting Behavior of Aqueous Cationic Surfactant Solutions on Liquid Films. *Langmuir* **2004**, *20*, 7575−7582.

(37) Thiele, U.; Todorova, D. V.; Lopez, H. Gradient Dynamics Description for Films of Mixtures and Suspensions: Dewetting Triggered by Coupled Film Height and Concentration Fluctuations. *Phys. Rev. Lett.* **2013**, *111*, 117801.

(38) Novotny, V. J.; Marmur, A. Wetting autophobicity. *J. Colloid Interface Sci.* **1991**, *145*, 355−361.

(39) Bera, B.; Duits, M. H. G.; Cohen Stuart, M. A.; van den Ende, D.; Mugele, F. Surfactant induced autophobing. *Soft Matter* **2016**, *12*, 4562−4571.

(40) Bera, B.; Carrier, O.; Backus, E. H. G.; Bonn, M.; Shahidzadeh, N.; Bonn, D. Counteracting interfacial energetics for wetting of hydrophobic surfaces in the presence of surfactants. *Langmuir* **2018**, *34*, 12344−12349.

(41) Marmur, A.; Lelah, M. D. The spreading of aqueous surfactant solutions on glass. *Chem. Eng. Commun.* **1981**, *13*, 133−143.

(42) Frank, B.; Garoff, S. Surfactant self-assembly near contact lines: control of advancing surfactant solutions. *Colloids Surf., A* **1996**, *116*, 31−42.

(43) Takenaka, Y.; Sumino, Y.; Ohzono, T. Dewetting of a droplet induced by the adsorption of surfactants on a glass substrate. *Soft Matter* **2014**, *10*, 5597−5602.

(44) Zhong, X.; Duan, F. Dewetting transition induced by surfactants in sessile droplets at the early evaporation stage. *Soft Matter* **2016**, *12*, 508−513.

(45) Tadmor, R.; Baksi, A.; Gulec, S.; Jadhav, S.; N'guessan, H. E.; Sen, K.; Somasi, V.; Tadmor, M.; Wasnik, P.; Yadav, S. Drops that change their mind: spontaneous reversal from spreading to retraction. *Langmuir* **2019**, *35*, 15734−15738.

(46) Kirkwood, J. G.; Riseman, J. The intrinsic viscosities and diffusion constants of flexible macromolecules in solution. *J. Chem. Phys.* **1948**, *16*, 565−573.

(47) Decker, E. L.; Frank, B.; Suo, Y.; Garoff, S. Physics of contact angle measurements. *Colloids Surf., A* **1999**, *156*, 177−189.

(48) Frank, B.; Garoff, S. Temporal and spatial development of surfactant self-assemblies controlling spreading of surfactant solutions. *Langmuir* **1995**, *11*, 4333−4340.

(49) Jarosiewicz, P.; Czechowski, G.; Jadżyn, J. The viscous properties of diols V. 1,2-hexanediol in water and butanol solutions. *Z. Naturforsch., A: Phys. Sci.* **2004**, *59*, 559−562.

(50) Karpitschka, S.; Riegler, H. Quantitative experimental study on the transition between fast and delayed coalescence of sessile droplets with different but completely miscible liquids. *Langmuir* **2010**, *26*, 11823−11829.

(51) Smit, B.; Schlijper, A. G.; Rupert, L. A. M.; van Os, N. M. Effects of chain length of surfactants on the interfacial tension: molecular dynamics simulations and experiments. *J. Phys. Chem.* **1990**, *94*, 6933−6935.

(52) Hu, J.; Xiao, X.-D.; Ogletree, D. F.; Salmeron, M. Imaging the condensation and evaporation of molecularly thin films of water with nanometer resolution. *Science* **1995**, *268*, 267−269.

(53) Huethorst, J. A. M.; Marra, J. Motion of Marangoni-Contracted Water Drops across Inclined Hydrophilic Surfaces. *Langmuir* **1991**, *7*, 2756−2763.

(54) Wijshoff, H. Drop dynamics in the inkjet printing process. *Curr. Opin. Colloid Interface Sci.* **2018**, *36*, 20−27.

(55) Bruning, M. A.; Costalonga, M.; Karpitschka, S.; Snoeijer, J. H. Delayed coalescence of surfactant containing sessile droplets. *Phys. Rev. Fluids* **2018**, *3*, 073605.

(56) Hansen, F. K.; Rødsrud, G. Surface Tension by Pendant Drop. *J. Colloid Interface Sci.* **1991**, *141*, 1−9.

(57) Fujiwara, H. *Spectroscopic Ellipsometry: Principles and Applications*; John Wiley & Sons, 2007; pp 158−177.